The 2013 World Congress on
Advances in Structural Engineering and Mechanics (ASEM13)
Jeju, Korea, September 8-12, 2013

Ultimate Bearing Capacity of Conical Shell Foundation

J.E. Colmenares[1)], So-Ra Kang[2)], Young-Jin Shin [3)] and *Jong-Ho Shin [4)]

[1)] *Dept. of Civil Eng, National University of Colombia, Bogota, Colombia*
[2)] *Development & Planning Dept. MidasIT, Kyoungki-do, Korea*
[3)] *DTS T-01 project, Samsung Construction and Trading Corporation, Abu Dhabi, UAE*
[4)] *Dept of Civil Eng, Konkuk University, Seoul, Korea*
[4)] *jhshin@konkuk.ac.kr*

ABSTRACT

Shell foundations have been employed as an alternative for the conventional flat shallow foundations and have proven to provide economical advantage. They have shown considerably improved performance in terms of ultimate capacity and settlement characteristics. However, despite conical shell foundations are frequently used in industry, the theoretical solutions for bearing capacity of these footings are available for only triangular shell strip foundations. The benefits in design aspects can be achieved through theoretical solutions considering shell geometry. The engineering behavior of a conical shell foundation on mixed soils was investigated experimentally and theoretically in this study. The failure mechanism was obtained by conducting laboratory model tests. Based on that, the theoretical solution of bearing capacity was developed and validated with experimental results, in terms of the internal angle of the cone. In comparison to the circular flat foundation, the results show 15% increase of ultimate load and 51% decrease of settlement at an angle of intersection of 120°. Based on the results, the design chart of modified bearing capacity coefficients for conical shell foundation is proposed.

1. INTRODUCTION

The structural and geometrical benefits of shell structures such as cylindrical,

hyper and conical shells have been well understood in structural engineering (Ghannad et al., 2012; Aghajari et al., 2011; Darilmaz, 2012). Recent research on conical shells investigating the effect of thickness variation and multi-layered composite has shown that the shell structure can be effectively optimized in terms of geometry and materials (Topal, 2013; Zerin, 2012).

The use of shell structures in foundation engineering has also drawn some interest, the reason being that shell foundations provide a higher bearing capacity, produce less settlement and are economical when compared to the conventional flat ones. Several studies have been performed together with experimental research for shell foundations with various geometries such as conical, hyper, concave and convex shells and cylindrical, triangular, folded plates (Szechy, 1965; Nicholls and Izadi, 1968; Kurian and Jeyachandran, 1972; Agarwal and Gupta, 1983). Numerical simulation have also been carried out to investigate various effects of involved parameters such as shell geometry, soil types, depth of embedment and material properties of soils (Jain et al. , 1977; Hanna and Abdel-Rahman, 1994; Kurian and Jayakrishna Devaki, 2001).

All the results indicate the general superiority of shell foundations, with respect to flat shallow foundations, based on the diverse interactions between soil and footings owing to their geometries.

Since Terzaghi (1943) proposed a well-conceived theory for determination of ultimate bearing capacity of shallow rough rigid foundation, many modifications and improvements have been made. To evaluate bearing capacity of shell foundations the classical bearing capacity solution for flat shallow foundations was extended, particularly for the triangular strip foundation (Hanna and Abdel-Rahman, 1990). Theoretical solution, however, should account for more various geometries of shell to appreciate the functional benefit in the design.

2. RUPTURE SURFACE FROM MODEL TESTS

In developing the theoretical formation in this study, the kinematic approach of limit analysis for a rough foundation was used to obtain solution to the bearing capacity. The main difficulty in this approach is related to the complexity of the mechanisms that can describe the process of failure reasonably well. Therefore the failure mechanism was experimentally investigated by model laboratory tests so that the upper bound solutions of the analysis can be applied based on the measured rupture surfaces. As

the failure modes were obtained physical model tests, it is assumed that the failure mechanism is exact. Thus the lower bound solution is not considered in this study. Tests were performed in two ways: first, tests for obtaining failure mode for half foundation section, and second, tests for obtaining load-settlement curves for full foundation section as shown in Figure 1.

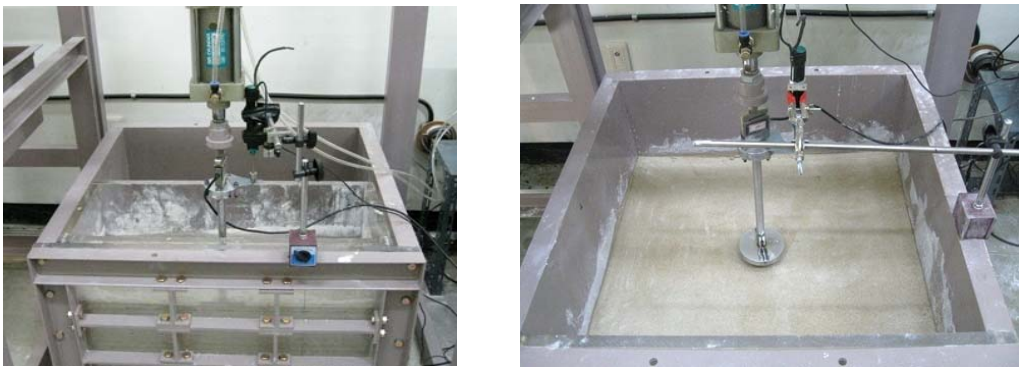

(a) rupture surface test(half section) (b) load - settlement test(full section)
Fig.1 Experimental set up

In order to catch a real rupture surface, an experimental setup was organized to perform a testing program as shown in Figure 1(a). A testing tank was made of acrylic panels and rigid steel frame, and its inner dimensions were 700 x 700 x 500 mm for length, width and depth, respectively. Size of the tank was large enough to prevent boundary effects.

A half section acrylic tank was addressed in order to capture rupture surface of the soil in the vicinity of the footing. To prevent buckling or deformation during loading in the half section the loading cylinder was fixed to the wall (see Figure 1(a)). Transparent and frictionless sheets with negligible stiffness were installed between the face of the soil tank and the soil mass.

The soil used in the present experimental investigation was a mixture of high silica sand and Kaolinite. Practically, sand is assumed as cohesionless and clay as frictionless. However, natural in-situ soils where shallow foundations are constructed, tend to have both characteristics. Therefore, 90 % silica sand and 10 % Kaolinite were mixed and used to reflect an intermediate soil material. Particle size distribution and direct shear box tests were performed. Figure 2 shows the particle size distribution of the tested sand and compares it with that of 100 % high silica sand. It indicates that because fine particles are added, the cohesive characteristics will be present in the material. A soil placing technique

was developed. It involved, mixing the soil and water and placing the mixture in layers of 2 cm thickness. It was followed by compaction, and pouring a thin colored shallow sand layer, which enables to identify the rupture surface. The technique was calibrated and the reproducibility of the material conditions was ensured by measuring that a unit weight of 14.98 kN/m^{3}was produced. The corresponding frictional angle and cohesion were 26.47° and 16.15 kN/m^2, respectively. Figure 2 summarizes the mechanical properties of the soil used. Pouring and compaction processes were repeated until the expected foundation level was reached. Voids in the cone shell were filled with the soils having the same void ratio.

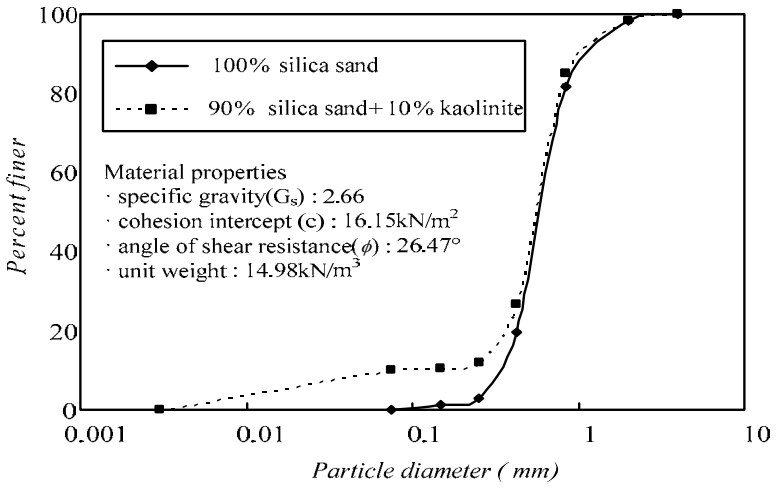

Fig.2 Grain size distribution and material properties

Four conical shapes of footing were used as shown in Figure 3. All the models had the same diameter B of 100 mm, length L of 55 mm, and the angle of intersection θ' varies from 90° to 180°. After the test was set up, a vertical load was applied under a displacement controlled rate of 1~ 2mm/min. The test was carried out up to failure and the deformation of surrounding soil was observed and photographed.

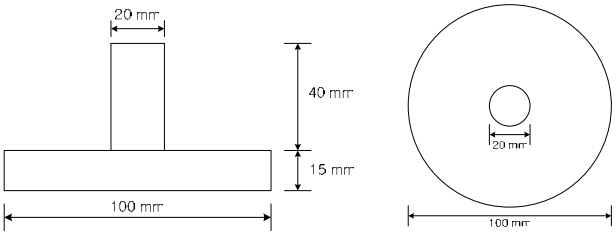

(a) flat circular footing (180° conical shell)

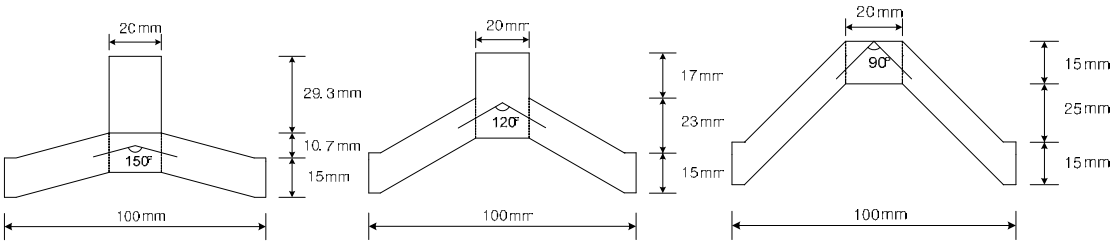

(b) 150° conical shell (c) 120° conical shell (d) 90° conical shell

Fig. 3 Models of conical shell footing

Figure 4 shows how the deformation results come up with a rupture surface. Coming along the colored layers in the soil, the vectors of deformed shape are drawn by the grid analysis and the rupture surface is identified. Several loading tests were performed before the testing in order to check the repeatability of the results. Rupture surfaces were identified by investigating relative movements of thin colored layers after large displacements.

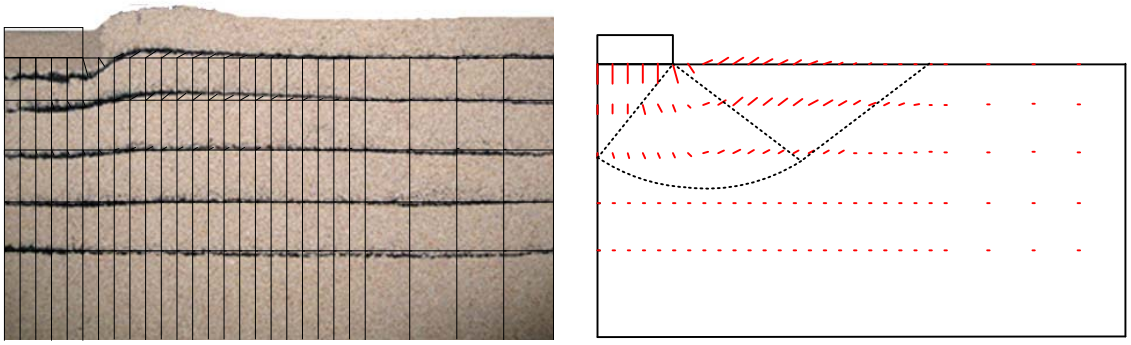

(a) pointing grids and deformation (b) drawing rupture surface

Fig. 4 Determination of rupture surface

As shown in Figure 5 theoretically the rupture surface for half section with the footing radius B` can be assumed to comprise of 3 zones: a triangular zone, a radial shear zone, and a Rankine`s passive zone indicating the angles of rupture surface ξ, θ, and η, respectively. The rupture surface stretched to H` vertically and L` horizontally.

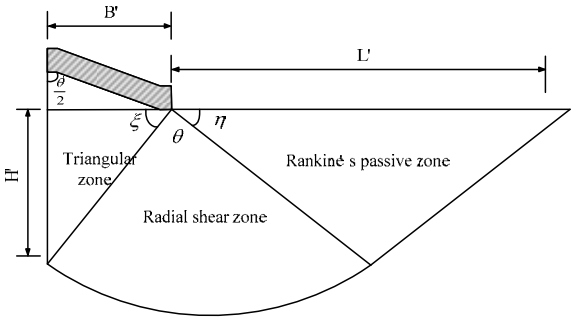

Fig. 5 Zonation of a rupture surface

There is no method to fully validate the failure mechanisms. Circular flat foundations of which failure mechanism is known can be considered as the special case of shell foundation. For circular flat foundation, Terzaghi (1943) proposed. $\xi = \pi/4 + \phi/4$, $\theta = \pi/2$, and $\eta = \pi/4 - \phi/4$ for $\phi = 26°$

Several attempts to reproduce the measures with the angles obtained from the equation were made by using the trial and error approach. The techniques validated from the circular models were applied to identify the rupture surface for other shells.

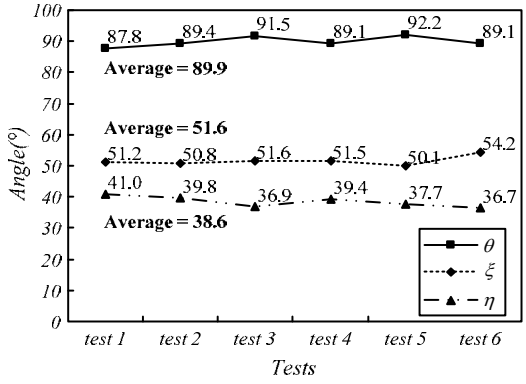

(a) 180° conical shell

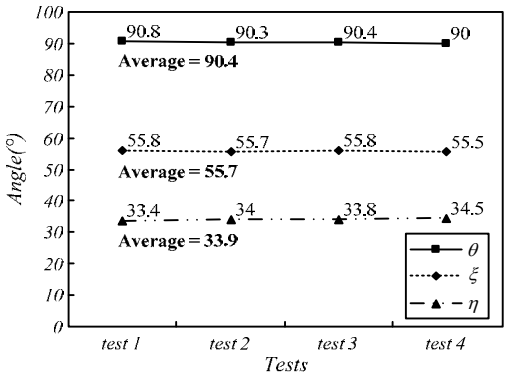

(b) 150° conical shell

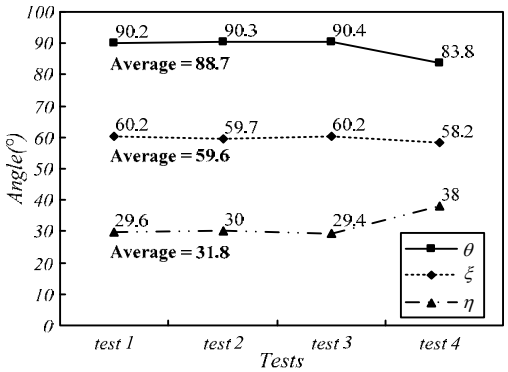

(c) 120° conical shell

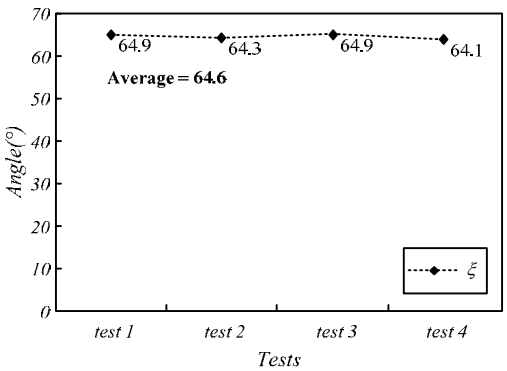

(d) 90° conical shell

Fig.6 Rupture surfaces of conical shell foundation

Figure 6 shows the angle of rupture surface for various conical geometries. The angles ξ, θ, and η were plotted with the angle of intersection θ', the angle ξ is relatively more sensitive to the change of angle of intersection than other angles. The angles θ barely change, and η seems to converge to a constant for the conical angle large than 120^o. Thus, it is assumed that both θ and η are constant for simplicity. The angle ξ increases when the angle of intersection decreases, θ', Hence, the relationship can be presented in Equation (10), with respect to angle of intersection, can be obtained from Figure 7

$$\xi = \frac{\pi}{4} + \frac{\phi}{4} + \beta \qquad (1)$$

where $\beta = (180° - \theta')/7$, ξ_c for the flat circular foundation, $\xi_c = \pi/4 + \phi/4$, ϕ is the internal friction angle of the ground, β is the increase of ξ respect to conical shape, and θ' is the angle of intersection of the conical shell foundation.

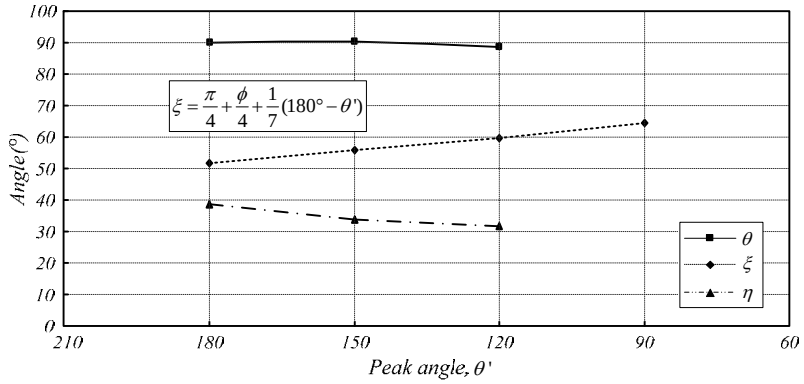

Fig.7 Effects of the conical angle of the shell

In the case of θ' = 90°, punch shear failure was observed, thus angles for radial shear zone and Rankine`s passive zone (θ and η) did not exist. The influencing ranges of rupture surfaces were given by the depth and width of rupture divided by the radius of footing respectively (L'/B' and H'/B'). As shown in Figure 8, the influencing range increases with decrease in angle of intersection except for θ' = 90° case. This indicates that the shell footings have a wider influencing range than the flat one. The area bounded by rupture surface is inversely proportional to the angle of intersection.

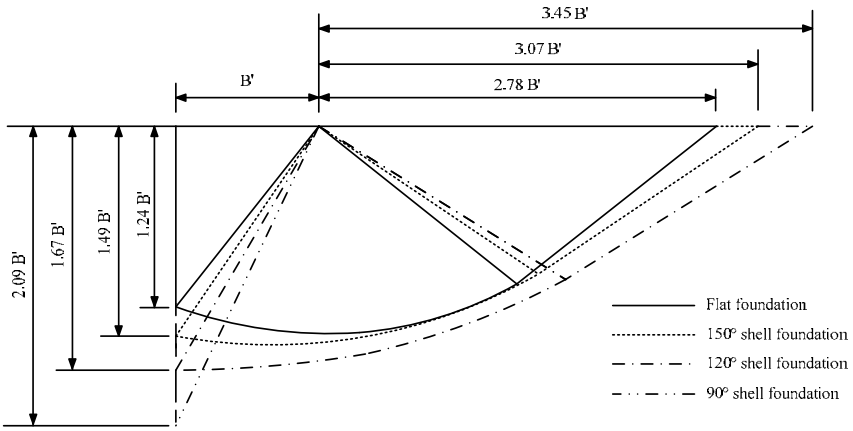

Fig.8 Comparisons of rupture surfaces

3. THEORETICAL STUDY

In this study, the theoretical solution of conical shell foundation was developed based on the failure mechanisms obtained from physical model tests. The rupture surface reflects the effect of conical shape. The upper bound solution of limit theorem was used: The rate of work dissipation within the soil mass as it deforms is not less than the work rate of external loads. It is also assumed that the soil conforms to the Mohr-Coulomb yield criterion and the deformation is governed by the normality rule. Figure 9 shows vertical cross-section of the failure mechanism. The soil beneath the shell foundation with diameter B (with radius $B = 2B'$ is subjected to a compressive loading, $q_u B$, and forms the deformation regions consisting of the triangular zone, the radial shear zone and the Rankine`s passive zone. The triangular zone $abc$ moves vertically with velocity $V_p$, followed by outward movement of radial shear zone and Rankine`s passive zone with velocities V_0, V_r, and V_q as shown in Figure 9. Line cd is a segment of log spiral, whose mathematical expression in polar coordinates, with respect to point a (in Figure 9 (a)), is given by Equation (3):

$$r = r_0 e^{\theta \tan\psi} \tag{3}$$

where r_o is equal to distance $\overline{ac}$, ψ is tangential angle at the plane of failure.

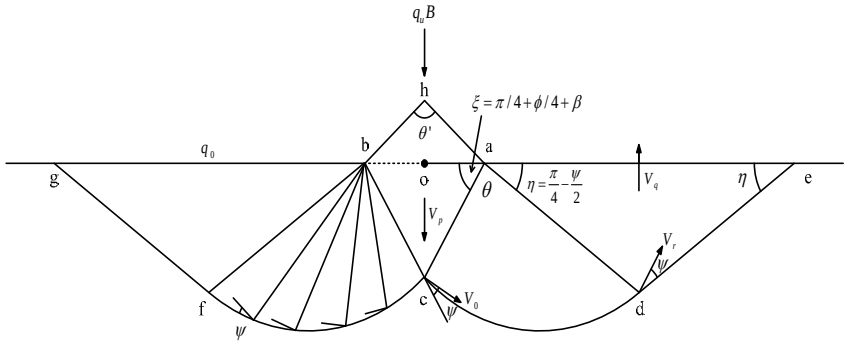

(a)

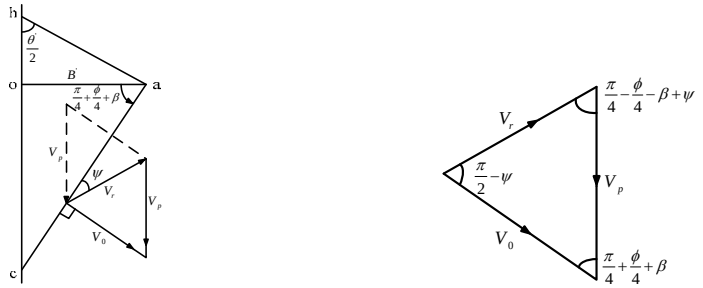

(b)

Fig. 9 Generalized failure mechanism

The velocity field in the cross section between $\overline{ac}$ and $\overline{ad}$ is uniform, therefore the magnitude of the velocity can be calculated:

$$V_r = V_0 e^{\theta \tan\psi} \tag{4}$$

Additionally the magnitude of velocities V_0, V_p, and V_r are expressed using sine principle as shown in Equation (5). See also Figure 9(b).

$$\frac{V_r}{\sin(\frac{\pi}{4}+\frac{\phi}{4}+\beta)} = \frac{V_0}{\sin(\frac{\pi}{4}-\frac{\phi}{4}-\beta+\psi)} = \frac{V_p}{\sin(\frac{\pi}{2}-\psi)} \tag{5}$$

$$V_r = \frac{V_0 \sin(\frac{\pi}{4}+\frac{\phi}{4}+\beta)}{\cos(\frac{\pi}{4}-\frac{\phi}{4}-\beta+\psi)},\ V_p = \frac{V_0 \cos\psi}{\cos(\frac{\pi}{4}+\frac{\phi}{4}+\beta-\psi)}$$

The lengths of $\overline{ac}$, $\overline{ad}$, $\overline{de}$, and $\overline{ae}$ can be derived as a function of the radius

B`, angles ϕ, β, and ψ:

$$\overline{ac} = \frac{B'}{\cos(\frac{\pi}{4} + \frac{\phi}{4} + \beta)} \tag{6}$$

$$\overline{ad} = \overline{de} = \overline{ac}\ e^{\theta \tan\psi} = \frac{B' e^{\theta \tan\psi}}{\cos(\frac{\pi}{4} + \frac{\phi}{4} + \beta)} \tag{7}$$

$$\overline{ae} = 2\overline{ad}\cos(\frac{\pi}{4} - \frac{\psi}{2}) = \frac{2B'\cos(\frac{\pi}{4} - \frac{\psi}{2}) e^{\theta \tan\psi}}{\cos(\frac{\pi}{4} + \frac{\phi}{4} + \beta)} \tag{8}$$

From the observed line $\overline{ae}$ and the angle β from the rupture surface in the experiment and referring Equation (8), the following relationship for ψ is empirically obtained for conical shells as

$$\psi = \frac{4}{11}\phi + \frac{1}{16}\beta \tag{9}$$

In order to derive the theoretical solution, the dissipation rate and the work rate of the soil weight are integrated over the entire volume of the mechanism, whereas the work rate of the given boundary stress and the limit load are integrated over their respective boundaries. Calculation is carried out first for footing on weightless soil.

The bearing capacity is presented as the sum of components dependent on the soil cohesion, surcharge and weight of soils:

$$q_u = f(c, q_o, \gamma \tag{10}$$

3.1 Weightless cohesion soil

Suppose that the contribution from cohesion is exclusively considered for the case of $c \neq 0, q_o = 0, \text{ and } \gamma = 0$, the dissipation rates in the 3 zones can be expressed:

① Internal energy dissipation including $\overline{ac}$

$$IW_{\overline{ac}} = c\pi \overline{oa}\,\overline{ac} V_r \cos\psi$$

$$= c\pi V_0 r_0^2 \frac{\sin(\frac{\pi}{4}+\frac{\phi}{4}+\beta)}{\cos(\frac{\pi}{4}+\frac{\phi}{4}+\beta-\psi)\cos(\frac{\pi}{4}+\frac{\phi}{4}+\beta)}\cos\psi \tag{11}$$

where, c is cohesion and r_0 is $\overline{ac}$.

② Internal energy dissipation in the shear zone (acd)

The dissipation rate in the radial shear zone accounts for varying log spiral and varying velocity in the zone by line integral:

$$c\int_0^\theta r\ Vd\theta = c\int_0^\theta \{r_0 e^{\theta\tan\psi}\}\{V_0 e^{\theta\tan\psi}\}d\theta = cr_0V_0\{\frac{e^{(\pi-\frac{\phi}{2}-2\beta+\psi)\tan\psi}-1}{2\tan\psi}\} \tag{12}$$

Figure 10 shows the infinitesimal increment taken into account:

$$\overline{aa'} = \overline{oa}\ dZ = r_0\cos(\frac{\pi}{4}+\frac{\phi}{4}+\beta)dZ \tag{13}$$

$$\overline{dd'} = \overline{o'd}\ dZ = \frac{\overline{od''}}{\cos(\frac{\pi}{4}-\frac{\psi}{2})}dZ = r_0\{\frac{\cos(\frac{\pi}{4}+\frac{\phi}{4}+\beta)}{\cos(\frac{\pi}{4}-\frac{\psi}{2})}+e^{(\frac{\pi}{2}-\frac{\phi}{4}-\beta+\frac{\psi}{2})\tan\psi}\}dZ \tag{14}$$

where, dZ is infinitesimal rotation.

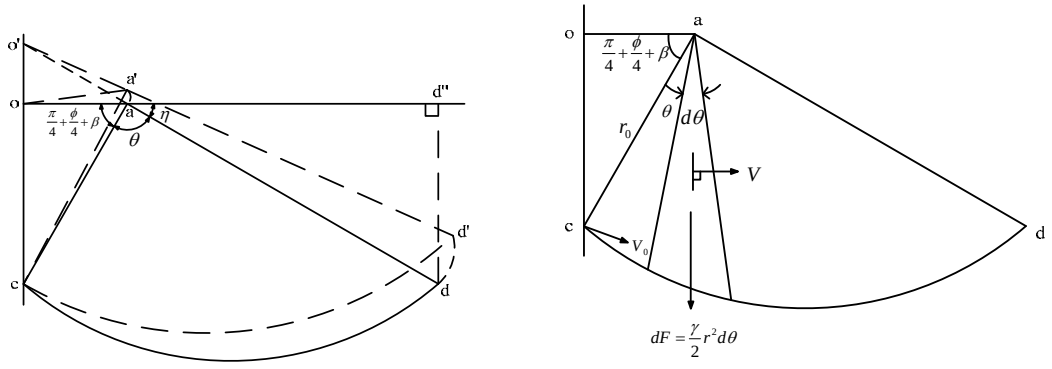

Fig. 10 The infinitesimal increment in the shear zone acd

It is integrated along the line $\overline{hc}$ from 0 to 2π for 3 dimensional expansion. Note that the infinitesimal increment is different at each point therefore the average infinitesimal displacement is adapted in Equation (15):

$$IW_{acd}=\int_0^{2\pi} cr_0V_0\{\frac{e^{(\pi-\frac{\phi}{2}-2\beta+\psi)\tan\psi}-1}{2\tan\psi}\}\frac{r_0}{3}\{\cos(\frac{\pi}{4}+\frac{\phi}{4}+\beta)+\frac{\cos(\frac{\pi}{4}+\frac{\phi}{4}+\beta)}{\cos(\frac{\pi}{4}-\frac{\psi}{2})}+e^{(\frac{\pi}{2}-\frac{\phi}{4}-\beta+\frac{\psi}{2})\tan\psi}\}dQ$$

$$=\frac{c\pi r_0^2\pi\cos(\frac{\pi}{4}+\frac{\phi}{4}+\beta)}{3\tan\psi}\{e^{(\pi-\frac{\phi}{2}-2\beta+\psi)\tan\psi}-1\}\{1+\frac{1}{\cos(\frac{\pi}{4}-\frac{\psi}{2})}+\frac{e^{(\pi-\frac{\phi}{2}-2\beta+\psi)\tan\psi}}{\cos(\frac{\pi}{4}+\frac{\phi}{4}+\beta)}\} \quad (15)$$

③ Internal energy dissipation in the passive zone (ade)

Figure 11 shows the infinitesimal increment of the Rankine`s passive zone. The dissipation rate in the passive zone can be calculated:

$$IW_{ade}=cV_r\pi\cos\psi\{\overline{oe}\,\overline{eo''}-\overline{od''}\,\overline{o''d}\}$$

$$=cV_r\pi\cos\psi\,2\overline{ad''}\{\overline{oa}+\frac{3}{2}\overline{ad''}\}\frac{1}{\cos(\frac{\pi}{4}-\frac{\psi}{2})}$$

$$=cV_0r_0^2\pi\cos\psi\{3\cos(\frac{\pi}{4}-\frac{\psi}{2})e^{(\frac{\pi}{2}-\frac{\phi}{4}-\beta+\frac{\psi}{2})\tan\psi}+2\cos(\frac{\pi}{4}+\frac{\phi}{4}+\beta)\}\times e^{(\pi-\frac{\phi}{2}-2\beta+\psi)\tan\psi} \quad (16)$$

④ External energy dissipation

When it comes to the external work from cohesion

$$EW_1=\pi q_u(\overline{oa})^2V_p$$

$$=\pi q_uV_0r_0^2\cos^2(\frac{\pi}{4}+\frac{\phi}{4}+\beta)\frac{\cos\psi}{\cos(\frac{\pi}{4}+\frac{\phi}{4}+\beta-\psi)} \quad (17)$$

where, q_u is ultimate bearing capacity.

The bearing capacity is then calculated from an energy rate balance equation considering all the deformed zones:

$$EW_1=IW_{\overline{ae}}+IW_{acd}+IW_{ade} \quad (18)$$

The coefficient of cohesion N_{cc} is obtained by rearranging the above equation as

$$q_u = cN_{cc} \tag{19}$$

Where, $N_{cc} = \tan(\frac{\pi}{4}+\frac{\phi}{4}+\beta)+\frac{\cos(\frac{\pi}{4}+\frac{\phi}{4}+\beta-\psi)}{3\cos(\frac{\pi}{4}+\frac{\phi}{4}+\beta)\sin\psi}\{e^{(\pi-\frac{\phi}{2}-2\beta+\psi)\tan\psi}-1\}$

$$\times\{1+\frac{1}{\cos(\frac{\pi}{4}-\frac{\psi}{2})}+\frac{e^{(\frac{\pi}{2}-\frac{\phi}{4}-\beta+\frac{\psi}{2})\tan\psi}}{\cos(\frac{\pi}{4}+\frac{\phi}{4}+\beta)}\}$$

$$+\frac{2\cos(\frac{\pi}{4}+\frac{\phi}{4}+\beta-\psi)e^{(\pi-\frac{\phi}{2}-2\beta+\psi)\tan\psi}}{\cos(\frac{\pi}{4}+\frac{\phi}{4}+\beta)}\times\{1+\frac{3\cos(\frac{\pi}{4}-\frac{\psi}{2})}{2\cos(\frac{\pi}{4}+\frac{\phi}{4}+\beta)}e^{(\frac{\pi}{2}-\frac{\phi}{4}-\beta+\frac{\psi}{2})\tan\psi}$$

3.2 consideration of surcharge

In the same manner, the contribution from surcharge is exclusively considered for the case of $c=0$, and $q\neq 0$. Assuming only the surcharge q_0 exists on $\overline{ae}$, the external work is obtained as follows:

$$EW_2 = \pi q_0(\overline{oe^2}-\overline{oa^2})V_q$$

$$= \pi q_0 4r_0^2 e^{(\frac{\pi}{2}-\frac{\phi}{4}-\beta+\frac{\psi}{2})\tan\psi}\cos(\frac{\pi}{4}+\frac{\psi}{2})\{\cos(\frac{\pi}{4}+\frac{\phi}{4}+\beta)+e^{(\frac{\pi}{2}-\frac{\phi}{4}-\beta+\frac{\psi}{2})\tan\psi}\cos(\frac{\pi}{4}+\frac{\psi}{2})\}V_q$$

$$= 4r_0^2 V_0 q_0\pi\cos(\frac{\pi}{4}+\frac{\psi}{2})\sin(\frac{\pi}{4}+\frac{\psi}{2})\{\cos(\frac{\pi}{4}+\frac{\phi}{4}+\beta)+\cos(\frac{\pi}{4}+\frac{\psi}{2})e^{(\frac{\pi}{2}-\frac{\phi}{4}-\beta+\frac{\psi}{2})\tan\psi}\}e^{2(\frac{\pi}{2}-\frac{\phi}{4}-\beta+\frac{\psi}{2})\tan\psi} \tag{20}$$

There is no internal dissipation in this case and the external work from bearing capacity is opposite to the work from the surcharge:

$$EW_1 - EW_2 = 0 \tag{21}$$

In this case, the coefficient of surcharge, N_{qc} is obtained:

$$q_u = q_0 N_{qc} \tag{22}$$

where,

$$N_{qc} = \frac{4\cos(\frac{\pi}{4}+\frac{\phi}{4}+\beta-\psi)}{\cos(\frac{\pi}{4}+\frac{\phi}{4}+\beta)}\{1+\frac{\cos(\frac{\pi}{4}+\frac{\psi}{2})}{\cos(\frac{\pi}{4}+\frac{\phi}{4}+\beta)}e^{(\frac{\pi}{2}-\frac{\phi}{4}-\beta+\frac{\psi}{2})\tan\psi}\}\times\cos(\frac{\pi}{4}+\frac{\psi}{2})\sin(\frac{\pi}{4}+\frac{\psi}{2})e^{2(\frac{\pi}{2}-\frac{\phi}{4}-\beta+\frac{\psi}{2})}$$

3.3 Consideration of soil weight

The influence of the soil weight on the bearing capacity is presented as an additional term:

$$q_u = \frac{1}{2}\gamma B N_{\gamma c} \tag{23}$$

where, $N_{\gamma c}$ are the bearing capacity coefficient of self-weight of shell foundation.

The bearing capacity coefficient $N_{\gamma c}$ ($c=0$, $q=0$, $\gamma \neq 0$) takes into account the self weight of ground under the footing including three soil clusters as follows:

① External energy including *ahoc*

From Figure 8, the external work is obtained:

$$\begin{aligned} EW_{ahoc} &= \frac{\pi}{3}\gamma \overline{oa^2}\{\overline{co}+\overline{oh}\}V_p \\ &= \frac{\pi}{3}\gamma\{r_0\cos(\frac{\pi}{4}+\frac{\phi}{4}+\beta)\}^2 r_0\{(\frac{\pi}{4}+\frac{\phi}{4}+\beta)+\cos(\frac{\pi}{4}+\frac{\phi}{4}+\beta)\cot(\frac{\theta'}{2})\}\frac{-V_0\cos\psi}{(\frac{\pi}{4}+\frac{\phi}{4}+\beta-\psi)} \\ &= \frac{\pi r_0^3 V_0\gamma}{2}h_1(\phi) \end{aligned} \tag{24}$$

where, $h_1(\phi) = -\frac{2}{3}\cos^3(\frac{\pi}{4}+\frac{\phi}{4}+\beta)\{\tan(\frac{\pi}{4}+\frac{\phi}{4}+\beta)+\cot(\frac{\theta'}{2})\}\frac{\cos\psi}{\cos(\frac{\pi}{4}+\frac{\phi}{4}+\beta-\psi)}$

② External energy including *acd*

From Figure 10, the external energy at *acd* can be expressed:

$$\int_0^\theta V\cos(\frac{\pi}{4}+\frac{\phi}{4}+\beta+\theta)\frac{\gamma}{2}r^2 d\theta = \frac{\gamma r_0^2 V_0}{2}\int_0^\theta e^{3\theta\tan\psi}V_0\cos(\frac{\pi}{4}+\frac{\phi}{4}+\beta+\theta)e^{\theta\tan\psi}\}d\theta \tag{25}$$

Integrating along the line $\overline{hc}$ from 0 to 2π for 3 dimensional expansion,

$$EW_{acd} = \int_0^{2\pi}\frac{\gamma r_0^2 V_0}{2(1+9\tan^2\psi)}[\{\cos(\frac{\pi}{4}+\frac{\psi}{2})-3\tan\psi\sin(\frac{\pi}{4}+\frac{\psi}{2})\}e^{3(\frac{\pi}{2}-\frac{\phi}{4}-\beta+\frac{\psi}{2})\tan\psi}$$

$$= \int_0^{2\pi}\frac{\gamma r_0^2 V_0}{2(1+9\tan^2\psi)}[\{\cos(\frac{\pi}{4}+\frac{\psi}{2})-3\tan\psi\sin(\frac{\pi}{4}+\frac{\psi}{2})\}e^{3(\frac{\pi}{2}-\frac{\phi}{4}-\beta+\frac{\psi}{2})\tan\psi}$$

$$-3\tan\psi\cos(\frac{\pi}{4}+\frac{\phi}{4}+\beta)-\sin(\frac{\pi}{4}+\frac{\phi}{4}+\beta)]\frac{r_0}{3}\{\cos(\frac{\pi}{4}+\frac{\phi}{4}+\beta)\}$$
$$+\frac{\cos(\frac{\pi}{4}+\frac{\phi}{4}+\beta)}{\sin(\frac{\pi}{4}+\frac{\psi}{2})}\frac{r_0}{3}\{\cos(\frac{\pi}{4}+\frac{\phi}{4}+\beta)+\frac{\cos(\frac{\pi}{4}+\frac{\phi}{4}+\beta)}{\sin(\frac{\pi}{4}+\frac{\psi}{2})}+e^{(\frac{\pi}{2}-\frac{\phi}{4}-\beta+\frac{\psi}{2})\tan\psi}\}dQ$$
$$=\frac{\pi r_0^3 V_0\gamma}{2}h_2(\phi) \tag{26}$$

where, $h_2(\phi)=\frac{2\cos(\frac{\pi}{4}+\frac{\phi}{4}+\beta)}{3(1+9\tan^2\psi)}[\{1+\frac{1}{\sin(\frac{\pi}{4}+\frac{\psi}{2})}+\frac{e^{(\frac{\pi}{2}-\frac{\phi}{4}-\beta+\frac{\psi}{2})\tan\psi}}{\cos(\frac{\pi}{4}+\frac{\phi}{4}+\beta)}\}$

$$\times\{-3\tan\psi\cos(\frac{\pi}{4}+\frac{\phi}{4}+\beta)-\sin(\frac{\pi}{4}+\frac{\phi}{4}+\beta)\}$$
$$+\{1-3\tan\psi\tan(\frac{\pi}{4}+\frac{\psi}{2})\}\{1+\frac{e^{(\frac{\pi}{2}-\frac{\phi}{4}-\beta+\frac{\psi}{2})\tan\psi}}{\cos(\frac{\pi}{4}+\frac{\phi}{4}+\beta)}\}\cos(\frac{\pi}{4}+\frac{\psi}{2})e^{3(\frac{\pi}{2}-\frac{\phi}{4}-\beta+\frac{\psi}{2})\tan\psi}$$
$$+\cot(\frac{\pi}{4}+\frac{\psi}{2})e^{3(\frac{\pi}{2}-\frac{\phi}{4}-\beta+\frac{\psi}{2})\tan\psi}\{1+3\tan(\frac{\pi}{4}+\frac{\psi}{2})\tan\psi\}]$$

③ External energy including *ade*

According to Figure 11, the external energy at *ade* can be expressed:

$$EW_{ade}=\frac{\pi\gamma}{3}\cos(\frac{\pi}{4}+\frac{\psi}{2})\overline{dd''}\{(\overline{oe^2}+\overline{c'd^2}+\overline{oec'd})-(\overline{c'd^2}+\overline{oa^2}+\overline{oac'd})\}V_1$$
$$=\frac{\pi\gamma}{3}\cos\psi\{\overline{dd''}\times 2\overline{ae}(2\overline{oa}+3\overline{ad''})\}V_0e^{(\frac{\pi}{2}-\frac{\phi}{4}-\beta+\frac{\psi}{2})\tan\psi}\cos(\frac{\pi}{4}+\frac{\psi}{2})$$
$$=\frac{\pi\gamma}{3}[2r_0e^{2(\frac{\pi}{2}-\frac{\phi}{4}-\beta+\frac{\psi}{2})\tan\psi}\sin(\frac{\pi}{4}+\frac{\psi}{2})\cos(\frac{\pi}{4}+\frac{\psi}{2})\{2r_0(\frac{\pi}{4}+\frac{\phi}{4}+\beta)\}$$
$$+3r_0e^{(\frac{\pi}{2}-\frac{\phi}{4}-\beta+\frac{\psi}{2})\tan\psi}\}]V_0e^{(\frac{\pi}{2}-\frac{\phi}{4}-\beta+\frac{\psi}{2})\tan\psi}\cos(\frac{\pi}{4}+\frac{\psi}{2})$$
$$=\frac{\pi r_0^3V_0\gamma}{2}h_3(\phi) \tag{27}$$

where,

$$h_3(\phi)=\frac{8}{3}\sin(\frac{\pi}{4}+\frac{\psi}{2})\cos^2(\frac{\pi}{4}+\frac{\psi}{2})\{2\cos(\frac{\pi}{4}+\frac{\phi}{4}+\beta)+3\cos(\frac{\pi}{4}+\frac{\psi}{2})e^{(\frac{\pi}{2}-\frac{\phi}{4}-\beta+\frac{\psi}{2})\tan\psi}\}e^{2(\frac{\pi}{2}-\frac{\phi}{4}-\beta+\frac{\psi}{2})\tan\psi}$$

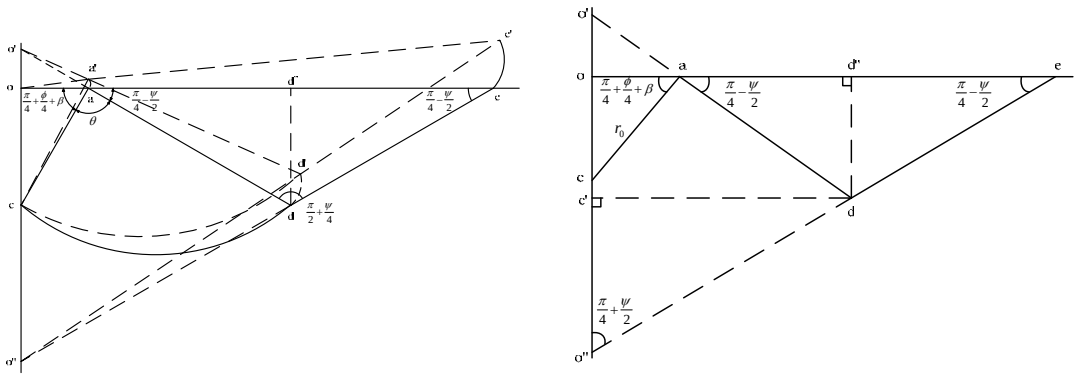

Fig. 11 The infinitesimal increment in the passive zone *ade*

There is also no internal dissipation in this case. Thus, the summation of external work from bearing capacity is zero:

$$EW_1 - (EW_{ahc} + EW_{acd} + EW_{ade}) = 0 \tag{28}$$

Therefore, the coefficient of self weight, $N_{\gamma c}$ is obtained as

$$N_{\gamma c} = \frac{\cos(\frac{\pi}{4}+\frac{\phi}{4}+\beta-\psi)}{2\cos^3(\frac{\pi}{4}+\frac{\phi}{4}+\beta)\cos\psi}[h_1(\phi)+h_2(\phi)+h_3(\phi)]$$

$$= \frac{1}{3}\{\tan(\frac{\pi}{4}+\frac{\phi}{4}+\beta)+\cot(\frac{\theta'}{2})\}+\frac{\cos(\frac{\pi}{4}+\frac{\phi}{4}+\beta-\psi)}{3\cos\psi\{1+9\tan^2\psi\}}\times[1-3\tan\psi\tan(\frac{\pi}{4}+\frac{\psi}{2})\}$$

$$\{1+\frac{e^{(\frac{\pi}{2}-\frac{\phi}{4}-\beta+\frac{\psi}{2})\tan\psi}}{\cos(\frac{\pi}{4}+\frac{\phi}{4}+\beta)}\}\cos(\frac{\pi}{4}+\frac{\psi}{2})e^{3(\frac{\pi}{2}-\frac{\phi}{4}-\beta+\frac{\psi}{2})\tan\psi}$$

$$+\{1+\frac{1}{\sin(\frac{\pi}{4}+\frac{\psi}{2})}+\frac{e^{(\frac{\pi}{2}-\frac{\phi}{4}-\beta+\frac{\psi}{2})\tan\psi}}{\cos(\frac{\pi}{4}+\frac{\phi}{4}+\beta)}\}\{3\tan\psi\cos(\frac{\pi}{4}+\frac{\phi}{4}+\beta)+\sin(\frac{\pi}{4}+\frac{\phi}{4}+\beta)\}$$

$$+\cot(\frac{\pi}{4}+\frac{\psi}{2})e^{3(\frac{\pi}{2}-\frac{\phi}{4}-\beta+\frac{\psi}{2})\tan\psi}\{1+3\tan(\frac{\pi}{4}+\frac{\psi}{2})\tan\psi\}]$$

$$+\frac{4\cos(\frac{\pi}{4}+\frac{\phi}{4}+\beta-\psi)}{3\cos^3(\frac{\pi}{4}+\frac{\phi}{4}+\beta)\cos\psi}\sin(\frac{\pi}{4}+\frac{\psi}{2})\cos^2(\frac{\pi}{4}+\frac{\psi}{2})$$

$$\{2\cos(\frac{\pi}{4}+\frac{\phi}{4}+\beta)+3\cos(\frac{\pi}{4}+\frac{\psi}{2})e^{(\frac{\pi}{2}-\frac{\phi}{4}-\beta+\frac{\psi}{2})\tan\psi}\}e^{2(\frac{\pi}{2}-\frac{\phi}{4}-\beta+\frac{\psi}{2})\tan\psi} \tag{29}$$

By combining Equation (19), (22) and (23), the general ultimate bearing capacity equation for the conical shell is obtained as

$$q_u = cN_{cc} + q_0 N_{qc} + \frac{1}{2}\gamma B N_{\gamma c} \tag{30}$$

where, N_{cc} , N_{qc}, and $N_{\gamma c}$ are the bearing capacity coefficients of cohesion, surcharge and self-weight, respectively. Based on the theoretical solution, charts of bearing capacity coefficients, N_{cc}, N_{qc}, and $N_{\gamma c}$ for conical shell foundation are made and shown in Figures 12. The coefficients are subject to the frictional angle ϕ and the angle of intersection θ' of shell geometry. This chart can be used for preliminary design. Further filed study would be required for design practice.

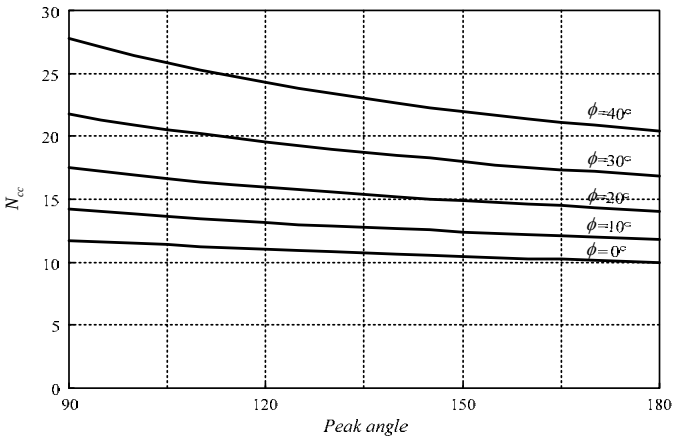

(a) N_{cc}

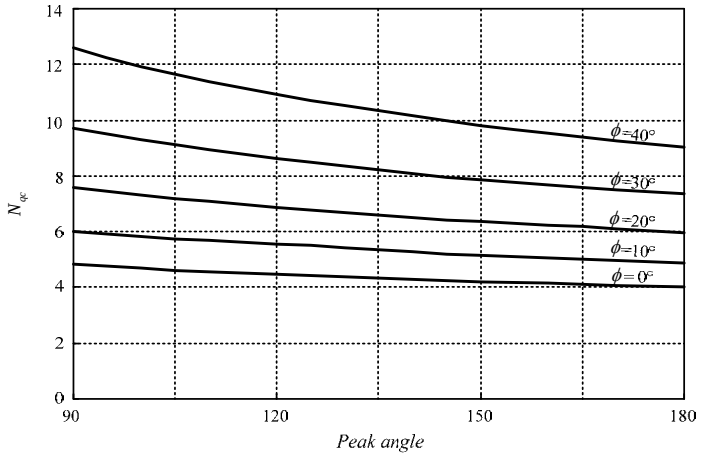

(b) N_{qc}

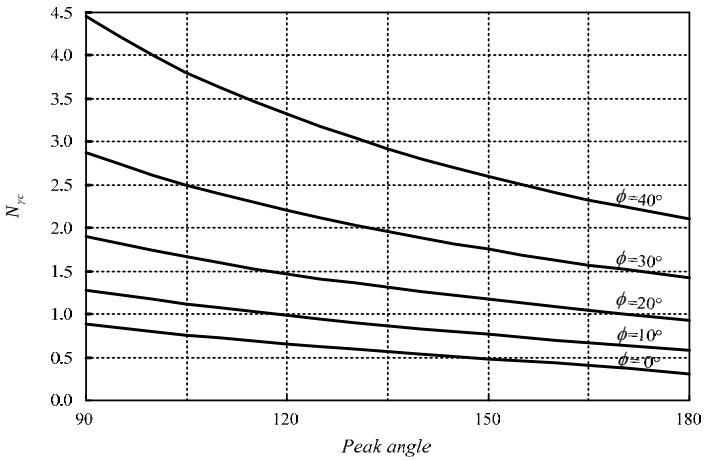

(c) $N_{\gamma c}$

Fig.12 Bearing capacity coefficients for conical shell foundations

4. EXPERIMENTAL VALIDATION

Load-settlement tests were carried out (Figure 1 (b)), and the results were compared with the theoretical solutions. Load-settlement relationships were recorded up to failure by a load cell and a linear variable displacement transducer (LVDT). The results are presented in Figure 13.

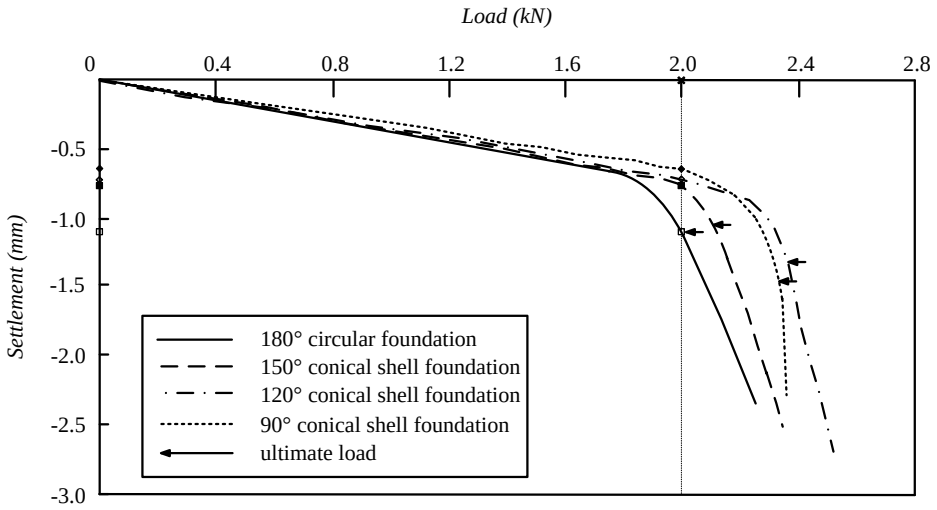

Fig.13 Load-settlement curves for the conical shell foundations

The ultimate load is defined as the point of maximum load obtained from

the curve at which the load starts decreasing while the settlement continues to increase. The ultimate loads obtained from the tests are 2.0 kN for 180^o shell and 2.11 kN for 150^o shell respectively. Table.1 compares the test results with theoretical solutions. Always theoretical results gave slightly higher values, however the differences are small.

Table. 1 Comparison experimental results with theoretical solutions

Cone Angle	Experimental Results(A) (kN)	Theoretical Results(B) (kN)	B/A
180	2.00	2.03	1.015
150	2.11	2.16	1.024
120	2.36	2.33	0.987
90	2.33	2.58	1.107

When compared with flat circular case, angle of intersection 150° and 120° achieve 7 % and 15 % increases of bearing capacity respectively. Angle of intersection 90° is not considered because a punching shear failure took place during the test. Settlement of the footings is inversely proportional to bearing capacity. It decreases up to 45 %, 51 % and 65 % compared with the settlement of flat circular case when the applied load is 2 kN (see Figure 13). It can be observed from these curves that conical shell foundations have higher ultimate loads and lower settlements than the conventional flat one.

5. CONCLUSIONS

Theoretical and experimental investigations on the ultimate bearing capacity of conical shell foundations on 10% Kaolinite-mixed sand were conducted. Theoretically, the classical solution of bearing capacity of a flat circular foundation was extended to the conical shell foundation. Upper bound solution of limit analysis was adopted. The results showed that conical shell foundations, in general, achieved a higher bearing capacity and a better settlement resisting characteristic than the conventional flat counterpart. In case of the conical angle of 120° the results presented 15% increase in ultimate load and 51% decrease in settlement. The smaller the angle of intersection of the foundation, the higher the

bearing capacity and the lower the measured settlement is. Tentative design charts for the modified bearing capacity coefficients for conical shell foundation were proposed in terms of internal friction angle of soil and the angle of intersection of the shell.

ACKNOLEDGEMENTS

The preparation of this paper was supported by the National Research Foundation of Korea under the research project 2012R1A2A1A01002326. The authors greatly appreciate the support provided. The first author also would like to thank to the Korea Foundation for Advanced Studies for its support carrying out the present study in Korea.

REFERENCES

Agarwal, K.B., and Gupta, R.N., 1983. “Soil-structure interaction in shell foundations”, In Proceedings of the International Workshop on Soil Structure Interaction, University of Roorkee, Roorkee, India. Vol.1, pp. 110-112.

Aghajari, S., Showkati H. and Abedi K. (2011), “Experimental investigation on the buckling of thin cylindrical shells with two-stepwise variable thickness under external pressure”. Structural Engineering and Mechanics, 39(6).

Darilmaz K. (2012), “Stiffened orthotropic corner supported hyper shells: Effect of stiffener location, rise/span ratio and fiber orientaton on vibration behavior”. Steel and Composite Structures, 12(4).

Ghannad, M. Zamani Nejad, M. Rahimi, G.H. and Sabouri, H. (2012) “Elastic analysis of pressurized thick truncated conical shells made of functionally graded materials”. Structural Engineering and Mechanics, 43(1).

Hanna, A., and Abdel-Rahman, M., 1990. "Ultimate bearing capacity of triangular shell strip footings on sand", Journal of Geotechnical Engineering, ASCE, 116: 1851-1863.

Hanna, A., and Abdel-Rahman, M., 1994. “Vertical displacement induced in soil by conical shell foundations", In Proceedings of the Conference on Vertical and Horizontal Deformations of Foundations and Embankments, ASCE, New York. Vol.2, pp. 937-948.

Hanna, A., and Abdel-Rahman, M., 1998. "Experimental investigation of shell foundations on dry sand", Canadian Geotechnical Journal, 35, pp. 847-857.

Jain, V.K., Nayak, G.C., and Jain, O.P., 1977. “General behavior of conical shell foundation” Proc. 3rd Int. Symp. Soil Structure Interaction, University of Roorkee, India, 2, pp. 53-61

Kurian, N.P., and Jeyachandran, S.R., 1972. "Model studies on the behaviour of sand under two and three dimensional shell foundations", Indian Geotechnical Journal, 2(1), pp. 79-90.

Kurian, N.P., and Jayakrishna Devaki, V.M., 2001. "Analysis of the geotechnical performance of shell foundations", In Proceedings of Indian Geotechnical Conference, Indore, Vol.1, pp. 83-86.

Nicholls, R.L., and Izadi, M.V. 1968. Design and testing of cone and hyper footings. Journal of Soil Mechanics and Foundation Engineering, ASCE, 94(SM1), pp. 47-72

Szechy, C., 1965. "The influence of shape of contact surface upon the bearing capacity and settlement of strip foundations", In Proceedings of the 5th Symposium of the Civil and Hydraulic Engineering Department, Indian Institute of Science, Bangalore. Vol.3(C2), pp. 1-7.

Terzaghi, K., 1943. Theoretical Soil Mechanics, Wiley, New York.

Topal, U. (2013), “Pareto optimum design of laminated composite truncated circular conical shells”, Steel and Composite Structures, 14(4).

Zerin, Z. (2012), “The effect of non-homogeneity on the stability of laminated orthotropic conical shells subjected to hydrostatic pressure”. Structural Engineering and Mechanics, 43(1).